Xavier University of Louisiana
XULA Digital Commons

Faculty and Staff Publications

9-1-2017

Microstructure of Injection Moulding Machine Mould Clamping Mechanism: Design and Motion Simulation

Z. Jin

Y. Zhang

X. Wang

J. Williams

Z. Liu

See next page for additional authors

Follow this and additional works at: https://digitalcommons.xula.edu/fac_pub

 Part of the Chemistry Commons

Authors

Z. Jin, Y. Zhang, X. Wang, J. Williams, Z. Liu, Z. Huang, D. Falkner, G. Zhou, L. Dong, J. Zhuang, and Zhe Wang

CAAI Transactions on Intelligence Technology

Research Article

Microstructure of injection moulding machine mould clamping mechanism: design and motion simulation

ISSN 2468-2322
Received on 15th June 2017
Revised on 8th September 2017
Accepted on 15th September 2017
doi: 10.1049/trit.2017.0011
www.ietdl.org

Zhiming Jin[1], Yajun Zhang[1], Xinliang Wang[2], Jacob Williams[3,4], Zhen Liu[3], Zhongyuan Huang[5,6], D'Lauren Falkner[5], Gang Zhou[2], Liqun Dong[1], Jian Zhuang[1] ✉, Zhe Wang[5]

[1]*College of Mechanical and Electrical Engineering, Beijing University of Chemical Technology, Beijing 100029, People's Republic of China*
[2]*Ningbo L.K. Technology Co. Ltd, Ningbo Zhejiang 315806, People's Republic of China*
[3]*Department of Physics and Engineering, Frostburg State University, Frostburg, MD 21532, USA*
[4]*Department of Mechanical Engineering, University of Maryland, College Park, MD 20742, USA*
[5]*Chemistry Department, Xavier University of Louisiana, New Orleans, LA 70125, USA*
[6]*College of Chemistry and Chemical Engineering, Xinyang Normal University, Xinyang, Henan 464000, People's Republic of China*
✉ *E-mail: zhuangjian@mail.buct.edu.cn*

Abstract: With the advent of intelligence technologies, more and more machines and devices are involved in the creation of complex structures. In the intelligent manufacturing industries, mouldings including injection moulding, blow moulding, compression moulding, and others play critical roles in manufacturing highly precise parts required for building intelligent machines (such as computers, cell phones, robots etc.). The performance of the clamping mechanism directly affects the quality of the microstructure of injection products. The design of the injection moulding mould clamping mechanism is based on the microstructure characteristics of the trip of the toggle lever mechanism ratio, speed ratio, and force amplification ratio. These are used to study the main performance parameters, such as analysis, as well as for the establishment of the physical model of the clamping mechanism. The model is based on the microstructure of injection of hyperbolic elbow clamping mechanism kinematics simulation. Simulation results and theoretical calculation contrast analysis show that the maximum dynamic template speed is 215.34 mm/s. The dynamic templates and cross-head speed ratio is 2.15; therefore, the design of the injection moulding mould clamping mechanism for the microstructure provides favourable technical support. The method described here is important to build complicated moulds required to build highly precise parts to build intelligent machineries.

1 Introduction

In recent years, microstructure injection moulding machines have been applied in optics, microfluidic devices, tiny medical instruments, micro-electro-mechanical system (MEMS) etc. [1–4]. The dimensions of micro injection molding products are usually on the scale of mg as weight unit and micron as length unit, or the surface microstructures of parts are micron-sized. Compared with the traditional injection moulding machine, the microstructure measuring injection volume and injection moulding machines must operate more accurately; therefore, more accurate clamping performance is required [5–9]. The microstructure of the injection moulding machine mainly adopts the hyperbolic elbow clamping mechanisms. Although a hyperbolic elbow structure has large clamping force, stress, high efficiency etc., it has articulated easy wear, the clamping force is not stable, the impact process is big, and the overall size is larger [10, 11]. Such intelligent system analysis and novel moulds development can offer advantages in new clap design, new injection design, new advanced control, integrated robotics, and precise process control.

In order to tackle the hyperbolic maximum elbow clamping mechanism defect, researchers conducted extensive research. Gao [12] using the five-point double toggle clamping mechanism motion characteristics and force analysis established a mathematical model with the target function theory, the maximum force amplifying ratio and the minimum overall axial size, and the parameters for design and motion simulation. Study and analysis by Zhang [13] of the toggle mechanism and influence of speed bit faster than the relevant parameters, a comprehensive analysis of the international market on the part of toggle clamping mechanism than the speed of the data puts forward the design optimisation of toggle mechanism of speed ratio curve and performance measures and methods. Under the condition of ignoring inertia force, Lin *et al*. [8] proposed a method to estimate the cross-head response to the thrust formula of clamping force. Zhong [7] built the toggle mechanism model, carried out the movement simulation, and verified the reliability and feasibility of the toggle mechanism, all of which will be designed and applied to the actual development to meet the performance requirements. Shao [14] has incorporated hybrid drive theory into the clamping mechanism design to design a servo motor and the conventional motor for the hybrid drive mode locking mechanism, which enabled the kinematics simulation and optimisation design. Existing research efforts have improved the performance of the locking mechanism to a certain extent; however, the rationality of the structure and stability of the locking mechanism still need further optimisation and improvement.

Based on several aforementioned representative ingenious systems, the ultimate goal is to introduce effective techniques for the fabrication of microstructures with high precision at an efficient cost. This mission also relies on the sophisticated computational approaches for mechanisms design under rationalising the process of the mechanical system. Such rationalisation in complex mechanical motions can be synthesised by various building blocks. In addition, new materials, such as carbon materials [15], polymers [16–18], nanomaterials, and nanocomposites [19–22], play more and more important role in our lives, so it is significant to develop injection moulding machines with better performance and could be applied to new materials. In order to realise the intelligent machining and processing, the fundamental understanding of laws of mechanics/physics take on greater significance in the moulds development process. Key mechanical components such as toggle level, toggle

This is an open access article published by the IET, Chinese Association for Artificial Intelligence and Chongqing University of Technology under the Creative Commons Attribution License (http://creativecommons.org/licenses/by/3.0/)

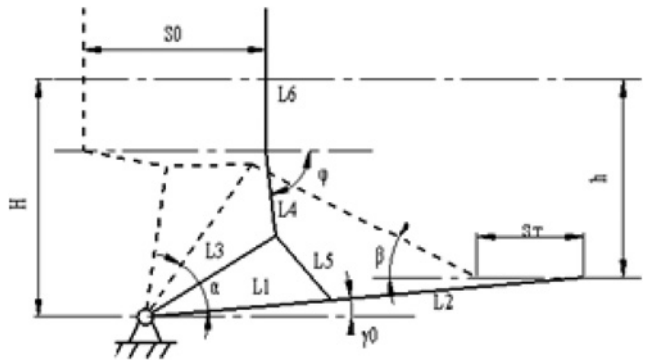

Fig. 1 *Toggle lever mechanism*

mould mechanism, locking and clamping etc., can indeed affect system reliability and promote higher processing performance. Novel moulds manufacturing can offer advantages to the next-generation machining process, with much higher reliability, performance, and sustainable operation.

In this study, the performance analysis of the mould clamping mechanism of the injection moulding machine based on the microstructure, stress, travel focus on double toggle clamping mechanism, speed ratio, and force amplifying ratio of main performance parameters are calculated and analysed. Moreover, microstructure injection moulding machine clamping mechanism schematic design and theoretical analysis are presented.

2 Design and theoretical analysis of clamping mechanism for microstructure injection moulding machine

2.1 Toggle lever mechanism design and calculation

The performance of the locking mechanism will be directly related to the quality of the product. In order to realise the intelligent machining and processing, the fundamental understanding of laws of mechanics/physics take on greater significance in the moulds development process. The main performance index of the 500 kN locking mechanism of the clamping force, mould closing stroke 250 mm, maximum modulus and thickness of 250 mm.

Fig. 1 shows a five-hinged double toggle mechanism diagram, where the dotted line represents the toggle mechanism clamping starting position and the solid line shows the clamping position.

According to the toggle mechanism schematic drawing point configuration diagram of the elbow bar mechanism in Fig. 1, the solid line and dotted line graphs of the corresponding bars create an equal constraint, the dotted line clamping position of rod L_1 and L_2 adds the collinear constraint, rod L_6 has a vertical constraint, and rod L_2 and the dynamic template connecting terminal has a horizontal line applying the collinear constraint. The microstructure of the injection moulding machine design requires a clamping force of 500 kN, a mould closing stroke of 250 mm, a maximum modulus and thickness of 250 mm, as well as the design parameters of the elbow bar mechanism shown in Table 1.

2.2 Analysis of toggle mould mechanism

As shown in Fig. 1, the solid line represents the toggle mould mechanism in place of the bars and movable plate location. At the time the toggle rod L_1 and Dalian L_2 are collinear; the dynamic template reaches the limit position. The dotted line is the position of the toggle mechanism at any one time. S_0 is the cross-head displacement and S_T is the displacement of the movable template. According to the length and position of the geometry, the relationship between the cross-head travel and move mould board stroke is

Table 1 Toggle lever mechanism geometry size

Project	Symbol	Numerical value	Unit
before the song elbow length	L_1	158	mm
length of the big connecting rod	L_2	205	mm
after bending the elbow length	L_3	100.09	mm
length of the small connecting rod	L_4	88	mm
θ the corresponding edge	L_5	74.79	mm
cross-head height	L_6	188	mm
diagonal	γ_0	3.95	°
angle between the L_1 and L_3	θ	21.7	°
pivot point to the centre distance of the tail plate	H	225	mm
in the plate under reamed hole centre distance	h	200	mm

$$S_0 = L_3[\cos(\theta+\gamma_0) - \cos(\alpha+\theta+\gamma_0)] - \sqrt{L_4^2 - \left[H - \frac{L_6}{2} - L_3\sin(\theta+\gamma_0)\right]^2} + \sqrt{L_4^2 - \left[H - \frac{L_6}{2} - L_3\sin(\alpha+\theta+\gamma_0)\right]^2}. \quad (1)$$

The move mould board stroke and cross-head travel ratio is

$$M_s = \frac{S_T}{S_0}. \quad (2)$$

To ensure the template displacement S_T is equal to the move mould board stroke $S_{max} = 250$ mm, use MATLAB software to the parameters in the equation, the mould in place when the crank angle maximum $\alpha_{max} = 104.74°$, mould in place when the crankshaft angle α is 0. According to the length and position of the geometry, the relationship between the cross head travel and the move mould board stroke.

In order to move, the template displacement, S_T, must be equal to the mould board stroke, $S_{max} = 250$ mm. MATLAB software was used to substitute the parameters in the equation. When the mould is in its first position, the maximum crank angle, $\alpha_{max} = 104.74°$. When the mould is in its second position, the crankshaft angle is 0°. The cross head travel S0 is of 216.38 mm, and the maximum travel ratio is about 1.15.

2.3 Toggle lever mechanism speed than the analysis and calculation

Fig. 2 shows a toggle mechanism motion to an arbitrary position diagram. V_0 is the cross-head speed, and V_m is the moving plate speed. According to the instantaneous centre method, the instantaneous centre of the velocity of the small connecting rod for L_4 is F, and the former toggle L_1 instantaneous centre of velocity is A. Dalian rod L_2 instantaneous centre of velocity for the G spot, by the instantaneous centre method and geometric relations, is as follows:

$$\frac{V_E}{V_D} = \frac{EF}{DF} = \frac{\sin(\alpha+\theta+\gamma_0+\varphi)}{\cos\varphi}, \quad (3)$$

$$\frac{V_D}{V_C} = \frac{L_5}{L_1}, \quad (4)$$

CAAI Trans. Intell. Technol., 2017, Vol. 2, Iss. 3, pp. 101–108
This is an open access article published by the IET, Chinese Association for Artificial Intelligence and Chongqing University of Technology under the Creative Commons Attribution License (http://creativecommons.org/licenses/by/3.0/)

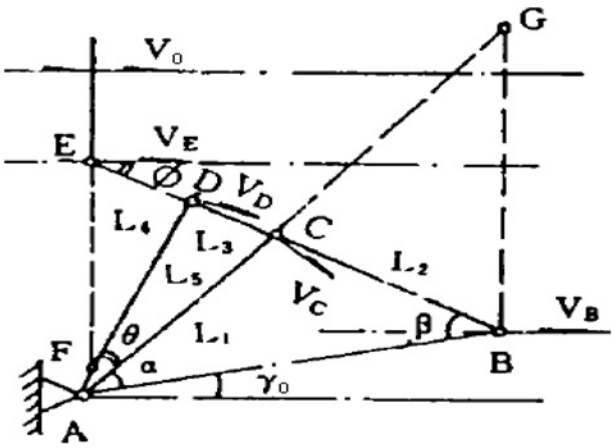

Fig. 2 *Toggle lever mechanism velocity analysis diagram*

$$\frac{V_B}{V_C}=\frac{GB}{GC}=\frac{\sin(\alpha+\beta+\gamma_0)}{\cos\beta}, \tag{5}$$

$$M_v=\frac{V_m}{V_0}=\frac{L_1\cos\varphi\sin(\alpha+\gamma_0+\beta)}{L_3\cos\beta\sin(\alpha+\gamma_0+\theta+\varphi)}. \tag{6}$$

The β angle and angle by the triangular relationship is given as

$$\beta=\arcsin\left[\frac{L_1}{L_2}\sin(\alpha+\gamma_0)-\frac{L_1+L_2}{L_2}\sin\gamma_0\right], \tag{7}$$

$$\varphi=\arcsin\frac{H-(L_6/2)-L_3\sin(\alpha+\theta+\gamma_0)}{L_4}. \tag{8}$$

The parameters in the above formula are as follows: in the mould begins, faster than M_v for the maximum, about 4.49, in the mould closing end faster than M_v 0. So, in the mould closing process, dynamic template motion law accords with slow–fast–slow requirements.

Substituting the parameters into the above formula results in faster than M_v for the maximum (about 4.49) as the mould begins faster than M_v (0) at the mould closing end. Therefore, in the mould closing process, the dynamic template motion law accords with slow–fast–slow requirements.

2.4 Amplification ratio analysis of elbow bar mechanism of force calculation

As shown in Fig. 3, F_0 is the cross-head screw thrust and F_c is the system deformation force and is equal to the cross-head thrust through the toggle mechanism amplified clamping force, F_m. The toggle mechanism sketch map is split into three parts. Fig. 3*a* is a cross-head force decomposition map, Fig. 3*b* is the dynamic template force decomposition map and Fig. 3*c* is the curved toggle force decomposition map, based on the static equilibrium relationship and geometric relations shown

$$F_0=2F_4\times\cos\varphi, \tag{9}$$

$$L_1\sin(\alpha+\gamma_0+\beta)=L_3\sin(\alpha+\theta+\gamma_0+\varphi), \tag{10}$$

$$F_4\times h_4=F_2\times h_2, \tag{11}$$

$$F_m=F_c=2F_2\times\cos\beta. \tag{12}$$

From the above formula

$$M_F=\frac{F_m}{F_0}=\frac{L_3\cos\beta\sin(\alpha+\gamma_0+\theta+\varphi)}{L_1\cos\varphi\sin(\alpha+\gamma_0+\beta)}. \tag{13}$$

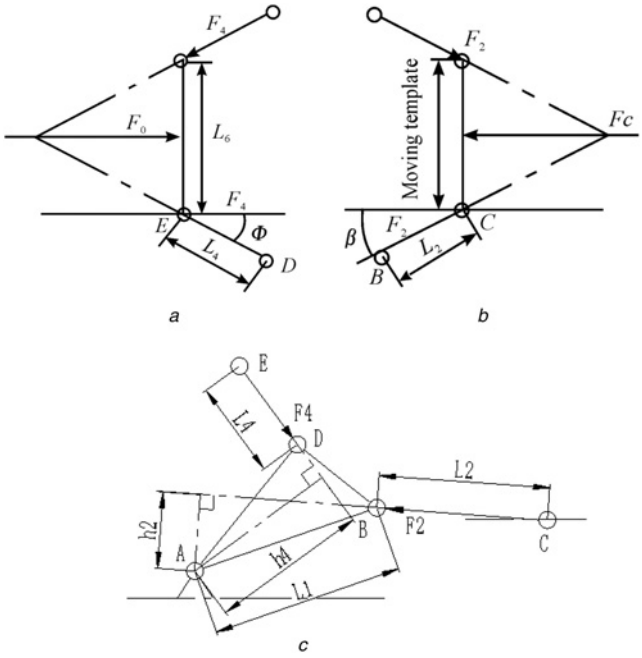

Fig. 3 *Toggle force diagram*

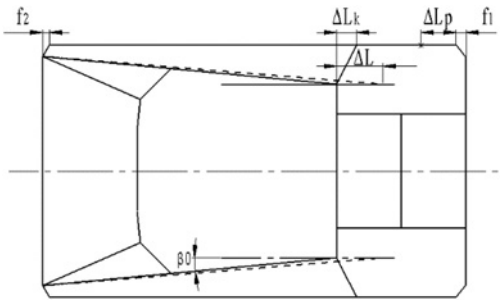

Fig. 4 *Schematic diagram of the mould clamping mechanism of deformation*

After substituting the parameters into the above formula, it is clear that the force-amplifying ratio increases with the decreasing crankshaft angle. When the crankshaft angle α is 3 DEG, the amplification ratio of force is 20.37. When the mould is in place, the crank angle α is 0°, the force-amplifying ratio is infinity, rods L_1 and L_2 are collinear, and the toggle mechanism is in a self-locking state. So in the mould closing fast in place, the cross-head only needs a small force to complete the mould closing action, and in the opening at the beginning, the cross-head also only needs a small force to complete the opening action.

2.5 Analysis system of deformation force calculation

In the process of mould closing in, gradually driving in the toggle mechanism template close to the front plate, when parting from the surface mould template and moving on to the front panel of the junction, the elbow angle α value reaches the critical angle α value of 0. As shown in Fig. 4, the pull rod L_p is elongated by ΔL_p, ΔL_k toggle is compressed, the clamping mechanism is elongated overall by ΔL, and the front plate and tail plate deflection are $f_1 f_q$, respectively. The first computing to design combined deformation mode force when rod. Then determine the clamping mechanism has started when the deformation position, namely elbow angle α value reaches the critical angle α_0 the main parameter values. Finally, get the formula for calculating the deformation force.

This is an open access article published by the IET, Chinese Association for Artificial Intelligence and Chongqing University of Technology under the Creative Commons Attribution License (http://creativecommons.org/licenses/by/3.0/)

By the following tensile elastic deformation formula:

$$\Delta L = \frac{FL}{ES}. \tag{14}$$

At the start deformation in the mold clamping mechanism, the dynamic template displacement is equal to the system of deformation. To make $C = (ES/L)$, $\Delta L = (F/C)$, therefore, the rod deformation is

$$\Delta L\mathrm{p} = \frac{F\mathrm{m}}{n_\mathrm{p} C\mathrm{p}}, \tag{15}$$

$$C_\mathrm{p} = \frac{E_\mathrm{p} S_\mathrm{p}}{L_\mathrm{p}}. \tag{16}$$

This leads to parameters $F_\mathrm{m} = 500$ kN, $N_\mathrm{p} = 1548.64$ mm, $S_\mathrm{p} = 2463.01$ mm^2, $E_\mathrm{p} = 2.1 \times 10^5$ N/mm^2, $N_\mathrm{p} = 4$, and $\Delta L_\mathrm{p} = 0.38$ mm.

2.6 Calculation of the critical angle $\alpha = 0$ system

The critical angle α_0 is a very important parameter of the toggle mechanism. The size of the clamping force is proportional to the size of the critical angle, and the clamping force size will affect the quality of products. Clamping force is small and the critical angle produces a smaller clamping force so that the mould cannot lock due to overflowing material or the product causes a flash. At smaller critical angles, the mechanism is unable to lock, affecting the performance of the mould clamping mechanism.

Through the deformation system in providing 500 kN clamping force under the circumstances to calculate bending, the elbow angle α reaches a critical angle α_0 when in the rod position. As shown in Fig. 4, the elbows L_1, L_2 do not consider the compressive deformation, and the tensile deformation of the rod system is equal to the tensile deformation, i.e. ΔL and ΔL_p.

As shown in Fig. 5, when considering the toggle mechanism of compressive deformation, L_1, L_2 in the role of the toggle system pressure under the shortened ΔL_1 and ΔL_2, the system will reduce the amount of stretch ΔL, ΔL_k, which can produce deformation of the rod for $\Delta L_\mathrm{p} = \Delta L - \Delta L_\mathrm{k}$. Therefore, in order to ensure the clamping force generated by the system for the 500 kN, by the calculation of =0.38 mm have L_p, $\Delta L = \Delta L_\mathrm{p} + \Delta L_\mathrm{k} = 0.38 + \Delta L_\mathrm{k}$. In Fig. 5, α_0, β_0, β, and γ_0 are considered to toggle compressive deformation values. α_{0a}, β_{0a}, β_a, and γ_{0a} toggle compressive deformation values were not considered. From Figs. 2–12, it can be obtained that $\alpha_o < \alpha_{oa}$, $\beta_o = \beta_{oa}$, $\beta < \beta_a$, $\gamma > \gamma_{oa}$

2.6.1 Deformation rod L_1, L_2 along with the long direction of the rod::

When the system starts to deform, toggle L_1, L_2 stress as shown in Fig. 6, P_c is the system of deformation force, by the compression deformation of ΔL_1 and ΔL_1. According to Fig. 6, L_1, L_2 along the rod length direction, respectively

$$\Delta L_1 = \frac{P_\mathrm{c}}{n_1 C_1 \cos(\alpha + \gamma_0)}, \tag{17}$$

$$\Delta L_2 = \frac{P_\mathrm{c}}{n_2 C_2 \cos\beta}, \tag{18}$$

$$C_1 = \frac{E_1 S_1}{L_1}, \quad C_2 = \frac{E_2 S_2}{L_2}. \tag{19}$$

The parameter γ_0 is unknown, γ_0 for clamping in place when L_1 and L_2 collinear L_1, L_2, and horizontal angle, γ_0 can be calculated by the following formula.

From Fig. 6, one can see that when clamping in place, $P_\mathrm{c} = F_\mathrm{m} = 500$ kN, $\alpha = 0$, β, $\gamma = 0$, L_1, L_2, and the compression deformation of ΔL_1, ΔL_2, are, respectively

$$\Delta L_1 = \frac{F_\mathrm{m}}{n_1 C_1 \cos\gamma_0}, \tag{20}$$

$$\Delta L_2 = \frac{F_\mathrm{m}}{n_2 C_2 \cos\gamma_0}, \tag{21}$$

Among them

$$\gamma_0 = \arcsin\frac{H - h}{L_1 - \Delta L_1 + L_2 - \Delta L_2}. \tag{22}$$

$E_1 = 2.09 \times 10^5$ N/mm^2, $E_2 = 1.62 \times 10^5$ N/mm^2, $S_1 = 2080$ mm^2, $S_2 = 5257.08$ mm^2, $n_1 = 4$, and $n_2 = 2$

For each parameter, (21), (22), and (23) were implemented in MATLAB, yielding the following solutions: $\Delta L_1 = 0.034$ mm, $\Delta L_2 = 0.06$ mm, $\gamma_0 = 3.95$, and the compression deformation length $L_1' = 158 - 0.034 = 157.96$ mm mould in place before the elbow and large rod, $L_2' = 205 - 0.06 = 204.94$ mm.

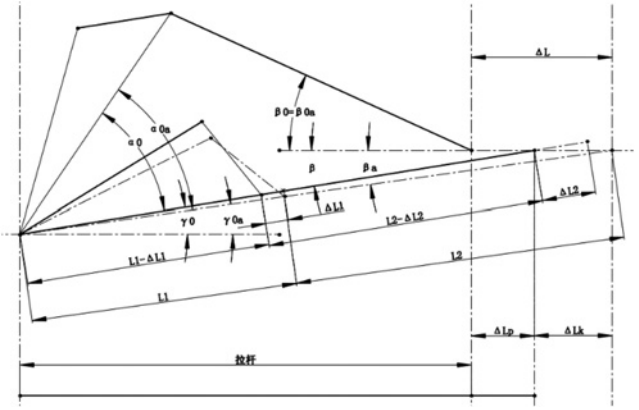

Fig. 5 *Toggle mechanism considering deformation of compression deformation*

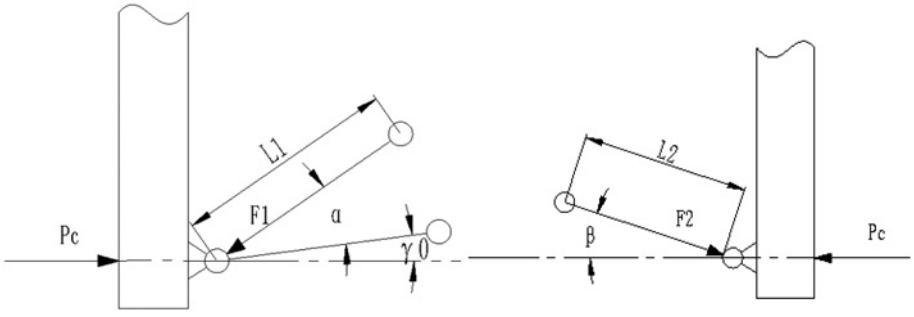

Fig. 6 *L_1, L_2 to toggle force diagram*

CAAI Trans. Intell. Technol., 2017, Vol. 2, Iss. 3, pp. 101–108
This is an open access article published by the IET, Chinese Association for Artificial Intelligence and Chongqing University of Technology under the Creative Commons Attribution License (http://creativecommons.org/licenses/by/3.0/)

2.6.2 Determination of the critical angle α_0: From Figs. 2–12 triangle available

$$(L_1' + L_2')\cos\gamma_0 - [L_1\cos(\alpha_0+\gamma_0) + L_2\cos\beta_0] = \Delta L_P, \quad (23)$$

$$\beta_0 = \arcsin\left[\frac{L'_1}{L'_2}\sin(\alpha_0+\gamma_0) - \frac{L'_1 + L'_2}{L'_2}\sin\gamma_0\right]. \quad (24)$$

Table 2 Toggle lever mechanism endpoint coordinates

Coordinate values	Coordinate values
A	(0, 0)
B	(157.62, 10.88)
C	(90.23, 43.32)
D	(362.14, 25)
E	(82.77, 131)
F	(82.77, 319)
G	(90.23, 406.68)
H	(0450)
I	(157.63, 439.12)
J	(362.14, 425)

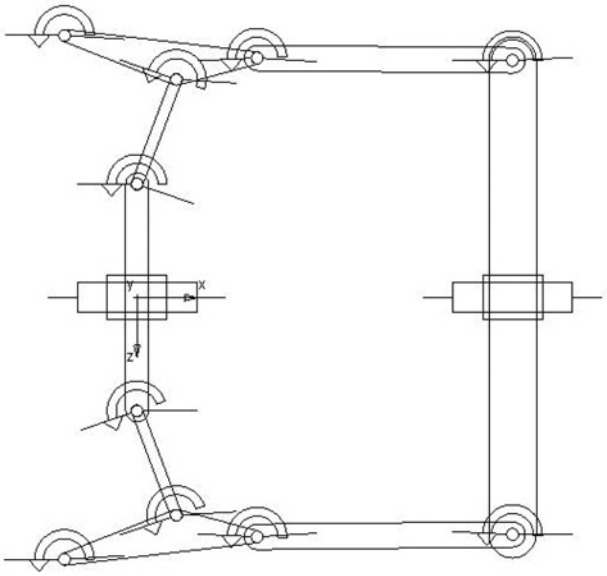

Fig. 7 *ADAMS simulation model of elbow bar mechanism*

To the known parameters, by formulae (15), (23), (24): $\alpha_0 = 3.32$ calculation.

3 Locking mechanism of ADAMS modelling

The establishment of the toggle mechanism is based upon a simplified model in ADAMS software. According to the closing position of each toggle mechanism is in place before die, bending the elbow L_1 and toggle the intersection of L_3 A for the origin, the calculated coordinates of each rod endpoint are shown in Table 2.

According to the structure of the toggle mechanism, geometry connected with each marker establishes the toggle mechanism. The geometry is relatively independent due to the need to establish the constraint relationship motion pair in order to establish various geometric bodies. According to the elbow movement form, add a rotating pair in each connecting rod hinge, with a total of 10. In the connecting rod cross-head of the representative 1 add them side relative to the ground. With respect to the moving platen toggle 2, add the mobile side relative to the ground. Get the mechanism of toggle mould in place when the model is as shown in Fig. 7. Fig. 7 represents toggle, Dalian 2 rod, 3 said the template, 4 said the small connecting rod, cross-head of 5 represents.

3.1 Clamping mechanism kinematics simulation

Applying linear clamping motion in the cross-head, speed is set to 100 mm/s, the simulation time is set to 2.5 s, and the simulation step number is set to 2500.The calculations of dynamic template displacement, cross-head displacement, and dynamic template velocity curves are shown in Fig. 8. The curves 1 and 2, respectively, are the dynamic template and cross-head displacement simulation curve, and curve 3 is the dynamic template speed simulation curve.

We can see from Fig. 8 that the moving plate displacement is 250 mm, cross-head displacement is 213 mm, and the trip is about 1.17, with those of theoretical calculation, meet the requirements. When the time is >1.2 s, the movable template gradually approaches the clamping position, the movable template speed gradually becomes smaller and eventually reduced to 0. However, as the applied cross-head speed is constant, so the speed curve of the initial value is not 0, not completely in line with the actual change template speed. In the actual movement, the cross-head speed at the beginning and the end stages of the process experience acceleration and deceleration. In order to simulate the actual motion process, as shown in Fig. 9, the 0–0.3 s cross-head speed was accelerated from 0 to 100 mm/s, the 0.3–2.1 s

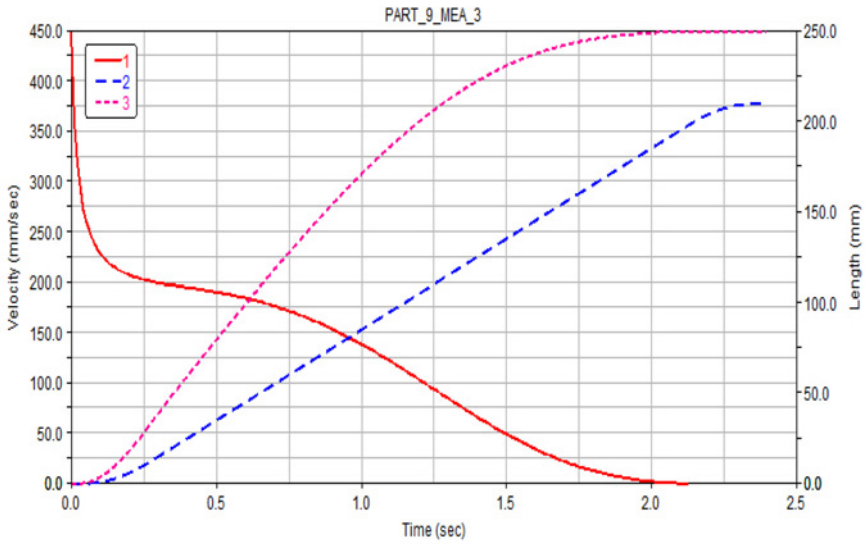

Fig. 8 *Dynamic template and cross-head simulation curve (1)*

This is an open access article published by the IET, Chinese Association for Artificial Intelligence and Chongqing University of Technology under the Creative Commons Attribution License (http://creativecommons.org/licenses/by/3.0/)

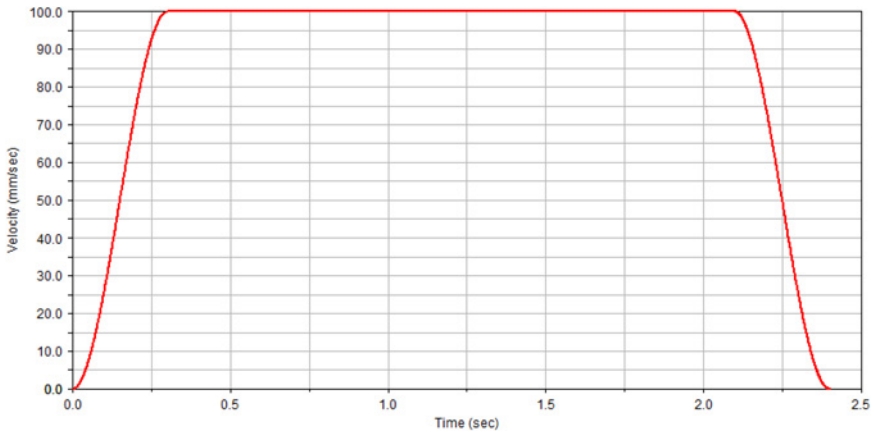

Fig. 9 *Cross-head application acceleration curve*

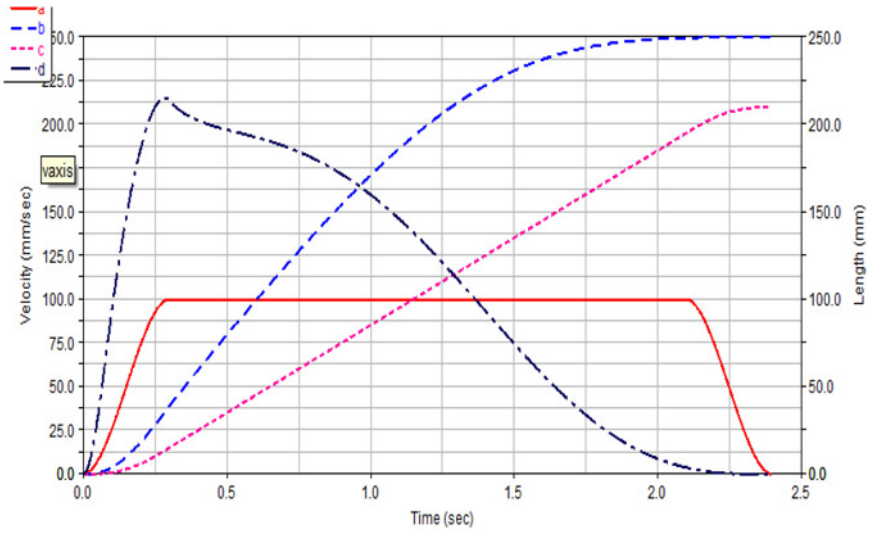

Fig. 10 *Dynamic template and cross-head simulation curve (2)*

cross-head followed uniform motion with a velocity of 100 mm/s, and from 2.1 to 2.4 s, the cross-head speed decelerated from 100 mm/s down to 0.

The simulation results shown in Fig. 10 show that in the beginning stages, dynamic template speed increases to the maximum value, and maintains high-speed movement.

When the mould is about to end, the movable template velocity decreases to the final 0. The dynamic changes of velocity template with slow–fast–slow speed requirements, which cause the change and displacement curve to be smooth with no mutation, help to reduce the dynamic template impact vibration phenomenon. The dynamic template maximum speed is 215.34 mm/s, and the rotating speed of the template and cross-head is 2.15.

3.2 Clamping mechanism dynamics simulation

When the dynamic template reaches the mold parting surface junction, the elbow angle α reaches the critical angle α_0, and clamping institutions begin to produce elastic deformation. Since the clamping force is equal to the magnitude of the deformation force of the pull rod clamping mechanism produced by the deformation of many factors, the decision to produce clamping force after moving template displacement by the toggle deformation, mould deformation etc. The simulation of mould clamping force, therefore, can use a spring to simulate the calculation of clamping force. A spring of elastic stiffness is equal to the system's total stiffness K, spring deformation ΔL is equal to the system, the type

$$\Delta L = \Delta L_{\mathrm{p}} + \Delta L_{\mathrm{k}}, \tag{25}$$

$$\Delta L_{2\mathrm{s}} = \Delta L_2 \times \cos\beta = \frac{F_{\mathrm{m}}}{n_2 C_2}. \tag{26}$$

This showed that $K = 1.068 \times 10^6$ N/mm and $\Delta L = 0.47$ mm. At the start of deformation in the mould clamping mechanism, the dynamic template displacement is equal to the system of deformation. When the distance between the spring starting position to the moving template position reaches 0.47 mm, and when the clamping mold is in place, the elbow angle α reaches the critical angle α_0. The location of the clamping mechanism beginning to deform is shown in Fig. 11.

When cross-head applied acceleration is 10 mm/s by uniform motion, the simulation results are shown in Fig. 12. When the crank angle value is less than the critical angle α_0, the locking mechanism begins deformation mould clamping force. As the elbow angle becomes smaller, the movable template gradually approaches the clamping position, and the clamping force becomes larger. When the mould is complete, i.e. elbow angle α is equal to 0, the mould closing force reaches the maximum value of 500 kN, which agrees with the theoretical calculation and design objectives.

CAAI Trans. Intell. Technol., 2017, Vol. 2, Iss. 3, pp. 101–108
This is an open access article published by the IET, Chinese Association for Artificial Intelligence and Chongqing University of Technology under the Creative Commons Attribution License (http://creativecommons.org/licenses/by/3.0/)

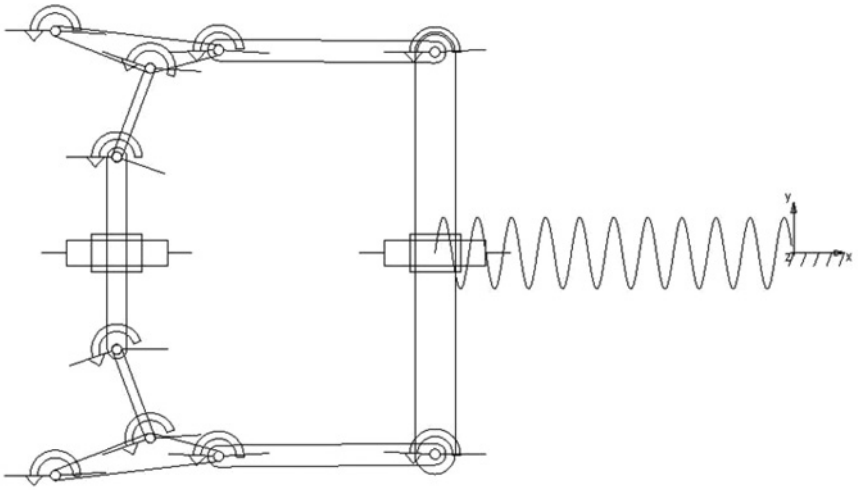

Fig. 11 *Clamping mechanism dynamics simulation model*

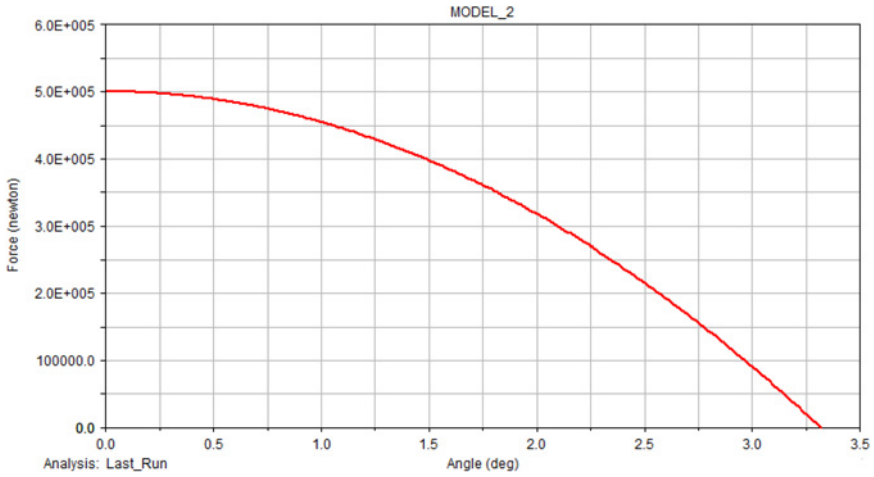

Fig. 12 *Clamping force simulation curve*

4 Conclusion

A mathematical model of the clamping mechanism is established to obtain the microstructure of the injection moulding machine stroke ratio of 1.15, faster than 4.49, force magnification ratio in crankshaft angle alpha is 3 DEG to 20.37. From the analysis of deformation of the locking mechanism, the diagonal and critical angle alpha 0 gamma 0 calculation equations were used to calculate the exact value: diagonal gamma 0 is 3.95°, critical angle alpha 0 is 3.32°. We obtained through dynamics simulation analysis dynamic template displacement of 250 mm and cross-head displacement of 213 mm. Through modifying cross-head speed function, dynamic template maximum speed is 215.34 mm/s, the moving speed of the template and the cross-head is 2.15. Finally, by setting spring, which represents the locking mechanism for dynamic simulation of elastic, the clamping mechanism of the deformation curve of mould clamping force, to the maximum value of 500 kN, which is consistent with the values, design target and theoretical calculation. Mould is a traditional subject but remaining advanced engineering challenges are governed by various mechanics/physics rules. Mathematical model design solutions have been conducted and applied for the development of injection molds, intelligent parts manufacturing used in robots, automates and other machineries. Also, with precise model design, the moulds can serve well with the multi-possibilities to achieve intelligent manufacturing. Such system analysis, modelling, and integration can ultimately serve the goal of developing next-generation intelligence machining such as intelligent sensing [23–26] and offer advanced mould design systems to fulfil the complexity of various industrial needs such as aircrafts, automotive, maritime parts etc.

5 Acknowledgments

This publication was made possible by funding from the National Science Foundation (HRD 1700429) and NIMHD-RCMI grant no. 5G12MD007595 from the National Institute of Minority Health, Health Disparities and the NIGMS-BUILD grant no. 8UL1GM118967.

6 References

[1] Packianather, M., Chan, F., Griffiths, C., *et al.*: 'Optimisation of micro injection moulding process through design of experiments', *Procedia CIRP*, 2013, **12**, pp. 300–305
[2] Liu, Z.Y., Loh, N.H., Tor, S.B., *et al.*: 'Binder system for micropowder injection molding', *Mater. Lett.*, 2001, **48**, (1), pp. 31–38
[3] Engleder, S.: 'Time-optimal motion planning and control of an electro hydraulically actuated toggle mechanism', *Mechatronics*, 2007, **17**, (8), pp. 448–456
[4] Sha, B., Dimov, S., Griffiths, C., *et al.*: 'Investigation of micro-injection moulding: factors affecting the replication quality', *J. Mater. Process. Technol.*, 2007, **183**, (2), pp. 284–296

This is an open access article published by the IET, Chinese Association for Artificial Intelligence and Chongqing University of Technology under the Creative Commons Attribution License (http://creativecommons.org/licenses/by/3.0/)

[5] Wang, G., Chen, H., Li, F.: 'Research on optimization design of double-toggle clamping unit for injection molding machine', *Eng. Plast. Appl.*, 2011, **39**, (5), pp. 87–90
[6] Huang, M.S., Lin, T.Y., Fung, R.F.: 'Key design parameters and optimal design of a five-point double-toggle clamping mechanism', *Appl. Math. Model.*, 2011, **35**, (9), pp. 4304–4320
[7] Attia, U.M., Marson, S., Alcock, J.R.: 'Micro-injection moulding of polymer microfluidic devices', *Microfluid. Nanofluid.*, 2009, **7**, (1), pp. 1–28
[8] Zheng, W.: 'Simulation analysis and experiment research of process in micro injection molding' (Dalian University of Technology, Dalian, 2006)
[9] Piotter, V., Guber, A., Heckele, M., *et al*.: 'Micro injection moulding of medical device component', *Bus. Brief., London: Med. Device Manuf. Technol.*, 2002, pp. 63–66
[10] Gao, D.Q., Guo, Z.G.: 'SimMechanics based on the injection molding machine and the optimization of design simulation', *Mach. Des. Manuf.*, 2009, (4), pp. 82–84
[11] Zhang, Y.G.: 'Researches on speed-transmission ratio of double-toggle clamping mechanism', *Beverage Ind.*, 2009, **12**, (9), pp. 34–41
[12] Lin, W.Y., Hsiao, K.M.: 'Investigation of the friction effect at pin joints for the five-point double-toggle clamping mechanisms of injection molding machines', *Int. J. Mech. Sci.*, 2003, **45**, (11), pp. 1913–1927
[13] Zhong, S.P.: 'Research on kinematics simulation of the double-toggle clamping mechanism for injection molding machine', *Equip. Manuf. Technol.*, 2010, (3), pp. 6–7
[14] Shao, Z.N., Ying, A.N., Xie, P.C., *et al*.: 'Design and optimization analysis for hybrid-drive clamping unit of all-electric injection moulding machine based on ADAMS software', *China Plast. Ind.*, 2010, **38**, (8), pp. 47–49
[15] Ameli, A., Kazemi, Y., Wang, S., *et al*.: 'Process-microstructure-electrical conductivity relationships in injection-molded polypropylene/carbon nanotube nanocomposite foams', *Compos. A: Appl. Sci. Manuf.*, 2017, (96), pp. 28–36
[16] Kumar, B., Doddamani, M., Zeltmann, S.E., *et al*.: 'Processing of cenosphere/HDPE syntactic foams using an industrial scale polymer injection molding machine', *Mater. Des.*, 2016, (92), pp. 414–423
[17] Aqeel, S.M., Huang, Z., Walton, J., *et al*.: 'Polyvinylidene fluoride (PVDF)/polyacrylonitrile (PAN)/carbon nanotube nanocomposites for energy storage and conversion', *Adv. Compos. Hybrid Mater.*, 2018, **1**, (1), pp. 185–192, DOI: 10.1007/s42114-017-0002-5
[18] Wei, H., Gu, H., Guo, J., *et al*.: 'Significantly enhanced energy density of magnetite/polypyrrole nanocomposite capacitors at high rates by low magnetic fields', *Adv. Compos. Hybrid Mater.*, 2018, **1**, pp. 127–134, DOI: 10.1007/s42114-017-0003-4
[19] Kroschwald, F., Nagel, J., Janke, A., *et al*.: 'Gold nanoparticle layers from multi – step adsorption immobilised on a polymer surface during injection molding', *J. Appl. Polym. Sci.*, 2016, **133**, pp. 1–8
[20] Battisti, M.G., Friesenbichler, W., Duretek, I., *et al*.: 'Correlation between rheotens measurements and reinforcement of polymer nanocomposites in the injection molding compounder', *J. Phys., Conf. Ser.*, 2015, **602**, (1), pp. 1–8
[21] Zhang, W., He, X., Li, C., *et al*.: 'High performance poly (vinyl alcohol)/cellulose nanocrystals nanocomposites manufactured by injection molding', *Cellulose*, 2014, **21**, pp. 485–494
[22] Liu, Z., Huang, Z., Cheng, F., *et al*.: 'Efficient dual-site carbon monoxide electro-catalysts via interfacial nano-engineering', *Sci. Rep.*, 2016, **6**, pp. 1–11
[23] Alippi, C.: 'A unique timely moment for embedding intelligence in applications', *CAAI Trans. Intell. Technol.*, 2016, **1**, (1), pp. 1–3
[24] Jin, H., Chen, Q., Chen, Z., *et al*.: 'Multi-leap motion sensor based demonstration for robotic refine tabletop object manipulation task', *CAAI Trans. Intell. Technol*, 2016, **1**, (1), pp. 104–113
[25] Zhang, X., Gao, H., Guo, M., *et al*.: 'A study on key technologies of unmanned driving', *CAAI Trans. Intell. Technol*, 2016, **1**, (1), pp. 4–13
[26] Padhy, S., Panda, S.: 'A hybrid stochastic fractal search and pattern search technique based cascade PI–PD controller for automatic generation control of multi-source power systems in presence of plug in electric vehicles', *CAAI Trans. Intell. Technol.*, 2017, **2**, (1), pp. 12–25

This is an open access article published by the IET, Chinese Association for Artificial Intelligence and Chongqing University of Technology under the Creative Commons Attribution License (http://creativecommons.org/licenses/by/3.0/)